Cardiovascular Engineering and Technology, Vol. 2, No. 1, March 2011 *(© 2010)* pp. 2–14
DOI: 10.1007/s13239-010-0030-6

Development of a Physical Windkessel Module to Re-Create *In Vivo* Vascular Flow Impedance for *In Vitro* Experiments

ETHAN O. KUNG[1] and CHARLES A. TAYLOR[1,2]

[1]Department of Bioengineering, Stanford University, James H. Clark Center, 318 Campus Drive, E350B, Stanford, CA 94305, USA; and [2]Department of Surgery, Stanford University, Stanford, CA, USA

(Received 6 August 2010; accepted 5 November 2010; published online 20 November 2010)

Associate Editor Stephen B. Knisley oversaw the review of this article.

Abstract—To create and characterize a physical Windkessel module that can provide realistic and predictable vascular impedances for *in vitro* flow experiments used for computational fluid dynamics validation, and other investigations of the cardiovascular system and medical devices. We developed practical design and manufacturing methods for constructing flow resistance and capacitance units. Using these units we assembled a Windkessel impedance module and defined its corresponding analytical model incorporating an inductance to account for fluid momentum. We tested various resistance units and Windkessel modules using a flow system, and compared experimental measurements to analytical predictions of pressure, flow, and impedance. The resistance modules exhibited stable resistance values over wide ranges of flow rates. The resistance value variations of any particular resistor are typically within 5% across the range of flow that it is expected to accommodate under physiologic flow conditions. In the Windkessel impedance modules, the measured flow and pressure waveforms agreed very favorably with the analytical calculations for four different flow conditions used to test each module. The shapes and magnitudes of the impedance modulus and phase agree well between experiment and theoretical values, and also with those measured *in vivo* in previous studies. The Windkessel impedance module we developed can be used as a practical tool to provide realistic vascular impedance for *in vitro* cardiovascular studies. Upon proper characterization of the impedance module, its analytical model can accurately predict its measured behavior under different flow conditions.

Keywords—Windkessel, Vascular impedance, *In vitro* validation, Blood flow, Flow resistance, Flow capacitance, Flow impedance, Flow inductance, Boundary condition, Phantom outlet.

Address correspondence to Charles A. Taylor, Department of Bioengineering, Stanford University, James H. Clark Center, 318 Campus Drive, E350B, Stanford, CA 94305, USA. Electronic mail: taylorca@stanford.edu

INTRODUCTION

Computational fluid dynamics (CFD) is a powerful tool for quantifying hemodynamic forces in the cardiovascular system. In CFD simulations, realistic outflow boundary conditions are necessary to represent physical properties of the downstream vasculature not modeled in the numerical domain, and to produce physiologic levels of pressure.[15] While various types of boundary condition implementations exist,[2,5,7,12,13] previous studies showed that impedance-based boundary condition is the preferred approach for coupling wave reflections from the downstream vasculature into the numerical domain,[15] and that simple lumped-parameter model representations can provide realistic impedances similar to those provided by a more complicated method employing a distributed parameter model.[2] The Windkessel model, due to its simplicity and ability to provide physiologically realistic impedances,[10,14,16,18] is a practical method of prescribing suitable boundary conditions to the numerical domain in CFD simulations.

The Windkessel model is represented as a circuit containing lumped elements of resistance, capacitance, and inductance. Although these elements are more generally interpreted in an electrical system, there is a direct analogy between the governing equations of an electric circuit and those of a fluid system, where the fluid pressure, the fluid volume, and the volumetric flow rate directly parallels voltage, electrical charge, and electrical current, respectively. For example, the relationship between voltage and current related by electrical resistance as described by the equation $V = IR$, can be directly modified into $P = QR$ to describe the relationship between pressure and flow rate related by the fluid resistance.

1869-408X/11/0300-0002/0 © 2010 Biomedical Engineering Society

When used to mimic vascular impedances, associations exist between the lumped component values in a Windkessel model and *in vivo* physiological parameters. The resistance and inductance values are associated with the density and viscosity of blood, and with the geometry and architecture of the vasculature which are functions of both the anatomy and the vascular tone. The capacitance value is most affected by the physical properties and the vascular tone of the large arteries. Since the properties of blood, the blood vessel anatomy and physical properties, and the vascular tone do not vary significantly within the time frames of a cardiac cycle, it is the general practice to implement an analytical Windkessel model with fixed component values.

In order to validate CFD against experimental data, methods must be developed to reliably construct a physical model of the Windkessel boundary condition such that there is a direct parallel between the experimental setup and the CFD simulation. In this paper we present the theories, principles, practical design considerations, and manufacturing processes for physically constructing the resistance and capacitance components of a Windkessel impedance module. These methods enable the construction of Windkessel components with values that are predictable and constant throughout their operating ranges. We also present an analytical model that describes the physical Windkessel module, and incorporates an inductance to account for fluid momentum. We manufactured several resistance units and tested them independently in a flow loop to verify their operations. Windkessel modules that mimic the thoracic–aortic and renal impedances were then assembled and tested under physiologic pulsatile flow conditions, and experimental measurements were compared to analytical predictions of pressure and flow.

METHODS

Determining Target Windkessel Component Values

Target values to aim for in the design and construction of the Windkessel components must first be determined. The component value estimation may be performed using a basic three element Windkessel model consisting of a proximal resistor (R_p), a capacitor (C), and a distal resistor (R_d) as shown in Fig. 1. The target component values are those that would result in the desired pressure and flow relationship reflecting the particular vascular impedance to be mimicked. For a periodic flow condition, the pressure and flow is related by the equation in the frequency domain:

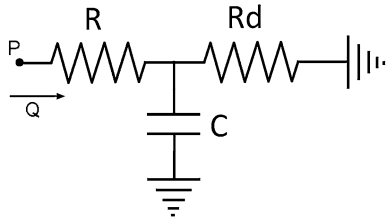

FIGURE 1. A basic three-element Windkessel model for component value estimation purpose.

$$P(\omega) = Q(\omega)Z(\omega) \tag{1}$$

where ω is the angular frequency, Q is the volumetric flow rate, and Z is the impedance of the three-element Windkessel circuit:

$$Z(\omega) = R_p + \frac{R_d}{1 + j\omega C R_d} \tag{2}$$

In previous reports, blood flow waveforms at various locations in the vascular tree have been obtained with imaging modalities such as ultrasound or phase-contrast magnetic resonance imaging,[1,3,9] and pressure waveforms have been obtained with pressure cuffs or arterial catheters.[8] Using the available *in vivo* flow and pressure waveform data, together with Eqs. (1) and (2), an iterative process can be performed to find the target Windkessel component values for mimicking the *in vivo* vascular impedance at a specific location. We begin by using the flow data and initial guesses of the component values as input parameter into Eqs. (1) and (2) to calculate a resulting pressure waveform. The component values can then be adjusted with the goal of matching the calculated pressure to the *in vivo* measured pressure waveform. For any given input flow, the total resistance (sum of R_p and R_d) can be adjusted to vertically shift the calculated pressure waveform, and the ratio of R_p/R_d as well as the capacitance can be adjusted to modulate the shape and pulse amplitude of the calculated pressure waveform. Once we determine the component values which give the desired pressure and flow relationship, we then consider them the target values in the design and construction of the components.

Flow Resistance Module

Theory and Construction Principles

In Poiseuille's solution for laminar flow in a straight cylinder, the relationship between the pressure drop

across the cylinder (ΔP) and volumetric flow rate (Q) is:

$$\Delta P = \frac{8\mu l}{\pi r^4} Q \tag{3}$$

The flow resistance defined as $R = \Delta P/Q$ is then:

$$R = \frac{8\mu l}{\pi r^4} \tag{4}$$

where μ is the dynamic viscosity of the fluid, l is the length of the cylinder, and r is the radius of the cylinder.

Equation (3) holds true in a laminar flow condition, where the resistance is constant and independent of flow rate. In turbulent flow, however, the additional energy loss leads to the pressure drop across the flow channel becoming proportional to the flow rate squared ($\Delta P \propto Q^2$), implying that the total effective resistance as defined by $R = \Delta P/Q$ is proportional to the flow rate ($R \propto Q$). Since the goal is to create a constant resistance that is independent of flow rate, it is thus important to avoid turbulence and maintain laminar flow. An approximate condition for laminar flow in a circular cylinder is the satisfaction of the following equation for Reynolds number:

$$\mathrm{Re} = \frac{vr}{\upsilon} = \frac{Q}{\pi \upsilon r} < 1200 \tag{5}$$

where v is flow velocity, r is the radius of the flow conduit, and υ is the kinematic viscosity of the fluid.

Equation (4) shows that with a single cylindrical channel of a given length, a high flow resistance can be achieved by drastically decreasing the cylinder radius. According to Eq. (5), however, decreasing the radius means that the flow conduit can only accommodate a lower flow rate while maintaining laminar flow. For physiological ranges of flows and impedances, it is generally the case that an R_p made from a single flow channel of a reasonable length would not be able to accommodate the required amount of flow. For example, the typical infra-renal aortic impedance results in an R_p of approximately 500 Barye s/cm^3, and the peak flow at that anatomical location is approximately 100 cc/s. Using a single cylindrical channel of length 10 cm, and a fluid kinematic viscosity of 0.04 g/cm s, the radius of such a resistor would be 0.22 cm. Equation (5) indicates that the maximum flow rate this resistor can accommodate in laminar flow condition is 33 cc/s, much less than the peak flow that will flow through it.

We present mathematically how such a problem can be overcome by using a large number of small channels in parallel, which simultaneously allows for high resistance and laminar flow at high flow rates. Consider "N" number of parallel flow channels with radius "r". We define:

A—combined cross sectional area of all channels
Q—combined volumetric flow through all channels
Q_{chan}—volumetric flow rate through each channel
Re—Reynolds number
R_{chan}—resistance of each channel
R_{total}—combined resistance of all the parallel channels.

The following two equations describe the geometry and resistances of the flow channels:

$$\frac{A}{N} = \pi r^2 \tag{6}$$

$$R_{total} = \frac{R_{chan}}{N} \tag{7}$$

From Eqs. (4), (5) and (6), we obtain the following proportionalities:

$$R_{chan} \propto \frac{1}{r^4} \tag{8}$$

$$A \propto \frac{Qr}{\mathrm{Re}} \tag{9}$$

$$r \propto \frac{1}{\sqrt{N}} \tag{10}$$

Substituting Eqs. (8) and (6) into Eq. (7)

$$R_{total} \propto \frac{1}{Ar^2} \tag{11}$$

Substituting Eq. (9) into Eq. (11)

$$R_{total} \propto \frac{\mathrm{Re}}{Qr^3} \tag{12}$$

Substituting Eq. (10) into Eq. (12) and re-arranging, we finally have

$$\frac{Q}{\mathrm{Re}} R_{total} \propto N^{3/2} \tag{13}$$

Equation (13) indicates that in order to achieve a high resistance at a high flow rate, while maintaining a low Reynolds number, a large number of parallel channels is required. Figure 2a is an illustration that shows the relationship between N and the maximum laminar flow rate for various values of R_{total}.

Practical Design and Construction Methods

To assemble a large number of small parallel channels in a practical and robust way, we placed

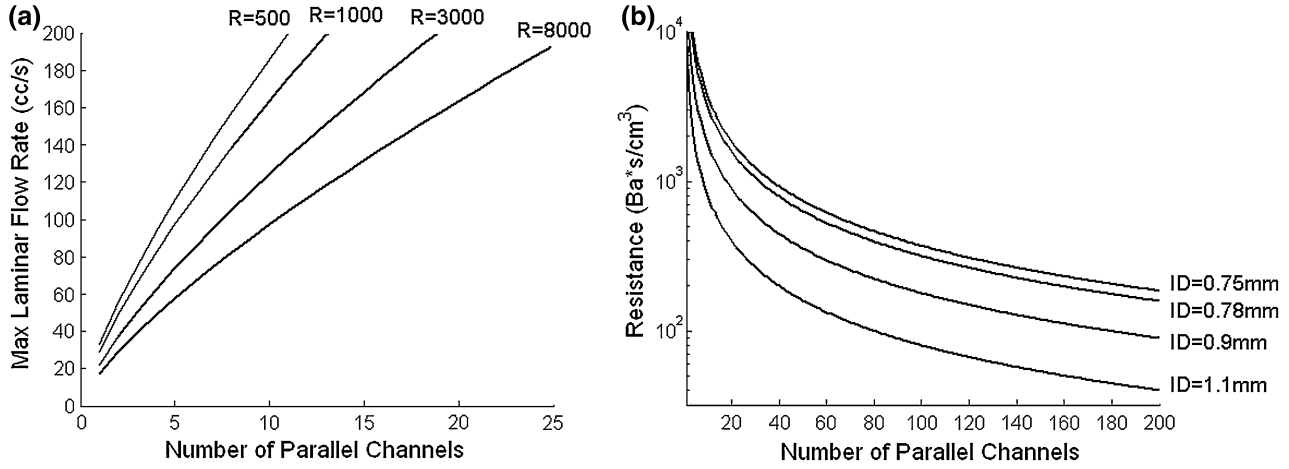

FIGURE 2. (a) Maximum laminar flow rate vs. number of parallel channels for various resistance values. (b) Resistance vs. number of parallel channels for various standard capillary tube inside diameters (ID). Calculated using: Fluid dynamic viscosity = 0.046 g/cm s. Capillary tube length = 10 cm.

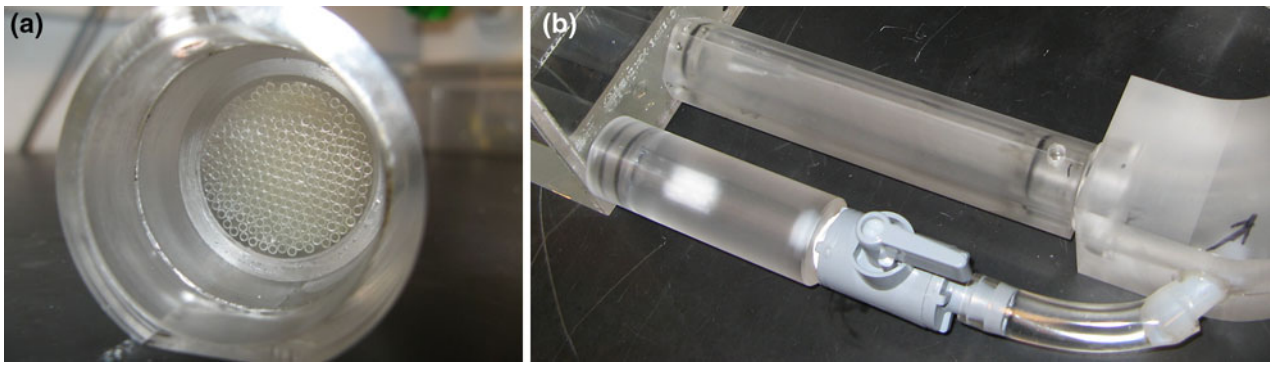

FIGURE 3. (a) Capillary tube resistance module construction. (b) Switchable resistance setup.

thin-walled glass capillary tubes (Sutter Instrument, CA) inside a plexiglass cylinder as shown in Fig. 3a. We applied a small amount of silicone rubber adhesive sealant (RTV 102, GE Silicones, NY) in between the capillary tubes around their middle section to adhere the tubes to one another, and to block fluid passageways through the gaps in between the tubes. We then applied a small amount of epoxy (5 Minute Epoxy, Devcon, MA) between the plexiglass surface and the bundle of capillary tubes to secure the capillary tubes inside the plexiglass cylinder.

The theoretical resistance of the resistance module is given by:

$$R = \frac{8\mu l}{\pi N r^4} \tag{14}$$

where μ is the dynamic viscosity of the working fluid, l is the length of the capillary tubes, r is the inside radius of each individual capillary tube, and N is the total number of capillary tubes in parallel.[17]

For a standard capillary tube length of 10 cm, Fig. 2b shows the relationship between the number of tubes and the resulting resistance for various standard capillary tube sizes that can be readily purchased.

Using the same principle of parallel channels, Fig. 3b shows a method for creating a switchable resistance module where the resistance value can be changed during an experiment. Multiple resistance modules can be placed in parallel, with control valves that open and close to add in or remove parallel resistor(s) in order to decrease or increase the effective total resistance.

The resistance module must be connected to tubing at each end. It is important to ensure that laminar flow is maintained throughout the connection tubing, and that diameter changes at the connection junctions are minimized to avoid the creation of turbulence. We constructed Table 1 to aid the design process of choosing an appropriate combination of a standard capillary tube size and connection tubing size, such that the resistance module can connect smoothly to its inlet and outlet tubing, and that the connection tubing itself can also accommodate the maximum flow rate required. The maximum laminar flow for any particular flow conduit diameter can be calculated from

TABLE 1. Estimated resistance values (and numbers of capillary tubes) resulting from various combinations of conduit diameter (maximum laminar flow rate), and capillary tube size.

Capillary tubes OD/ID[a] (mm)	1″ (200 cc/s)	3/4″ (150 cc/s)	5/8″ (125 cc/s)	1/2″ (100 cc/s)	3/8″ (75 cc/s)	1/4″ (50 cc/s)
2/1.56	231 (137)	410 (77)	591 (54)	923 (34)	1,641 (19)	3,693 (9)
1.5/1.1	525 (244)	934 (137)	1,345 (95)	2,101 (61)	3,735 (34)	8,404 (15)
1.2/0.9	750 (381)	1,334 (214)	1,920 (149)	3,000 (95)	5,334 (54)	12,002 (24)
1/0.78	923 (548)	1,641 (308)	2,364 (214)	3,693 (137)	6,566 (77)	14,773 (34)
1/0.75	1,080 (548)	1,920 (308)	2,765 (214)	4,321 (137)	7,681 (77)	17,282 (34)

Calculated using fluid dynamic viscosity = 0.046 g/cm s.
Fluid density = 1.1 g/mL.
Capillary tube length = 10 cm.
Circle packing density = 0.85 by area.
[a]OD/ID stands for outside diameter/inside diameter.

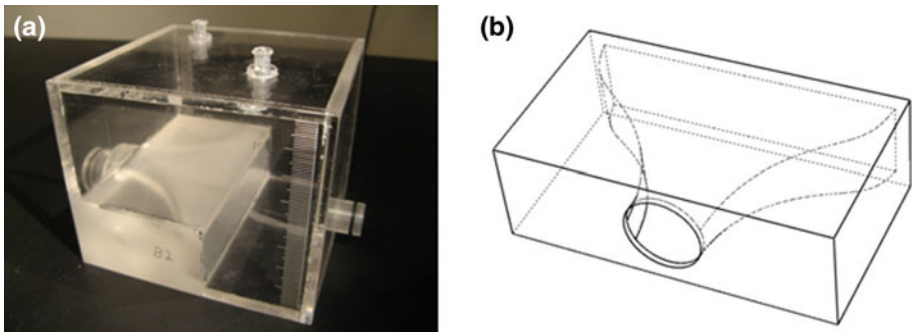

FIGURE 4. (a) Capacitance module construction. (b) Capacitor inlet contour.

Eq. (5), and is listed beside each conduit diameter in the table. Note that the Reynolds number within the capillary tubes is much lower than that in the connection tubing (due to the smaller diameter of the capillary tubes), thus the critical factor in maintaining laminar flow is the connection tubing diameter. From Table 1, the optimal capillary tube size for constructing the resistance module is determined by identifying a resistance value that is close to the desired target value, in combination with a conduit diameter that can accommodate the maximum expected flow. Once the capillary tube size is determined, a circle packing algorithm[11] can then be used to determine the precise plexiglass cylinder diameter required to house the specific number of capillary tubes needed for obtaining the desired resistance. Upon completing the actual construction of the resistance module, we manually count the number of capillary tubes in the plexiglass cylinder, and use the resulting count, together with the measured dynamic viscosity of the working fluid and Eq. (14), to determine the theoretical resistance of the module.

Flow Capacitance Module

The capacitance of a fluid system is defined as $C = \Delta V/\Delta P$ where ΔV and ΔP are the changes in volume and pressure. In a closed system at constant temperature, an ideal gas exhibits the behavior $PV = (P + \Delta P)(V - \Delta V)$, where P and V are the reference pressure and volume. The capacitance of a pocket of air is then:

$$C_a = (V - \Delta V)/P \tag{15}$$

We constructed the capacitance module with a plexiglass box that can trap a precise amount of air, which acts as a capacitance in the system (Fig. 4a). Equation (15) indicates that, as fluid enters the capacitor and compresses the air, the capacitance of the module would decrease. For small changes in volume relative to the reference volume, however, a reasonably constant capacitance can be maintained. As fluid enters and exits the box, the vertical level of the fluid in the box rises and falls slightly. The varying fluid level contributes to an additional capacitance that is in series with the capacitance due to air compression. The pressure change in the fluid due to the varying fluid level under the effects of gravity and fluid mass is:

$$\Delta P = \rho g \Delta h = \rho g \Delta V/A \tag{16}$$

where ρ is the fluid density, g is the gravitational constant, and A is the area of the fluid/air interface (assuming a column of fluid with constant

cross-sectional area). The capacitance due to the varying fluid level is then:

$$C_v = A/(\rho g) \tag{17}$$

Since C_v is in series with C_a the overall capacitance C can be approximated by C_a alone if $C_v \gg C_a$:

For $C_v \gg C_a$:

$$C = \left(\frac{1}{C_a} + \frac{1}{C_v}\right)^{-1} = \frac{C_a C_v}{C_a + C_v} \sim C_a \tag{18}$$

In the actual construction of the capacitance module, we designed the box to be large enough so that the approximation in Eq. (18) is true. We also designed a smooth contour for the inlet of the capacitance module (Fig. 4b) in order to minimize flow turbulences and thus avoid parasitic resistances. In addition, two access ports are included at the top of the capacitance module for air volume modulation and pressure measurements, and a graduated scale on the sidewalls for air volume measurement (Fig. 4a).

Flow Inductance

The flow inductance is an inherent parameter of a fluid system resulting from the fluid mass. It describes how a force, manifest as a pressure differential, is required to accelerate a body of fluid. The inductance in a fluid system creates a pressure drop in response to a change in flow as described by the equation:

$$\Delta P = L\frac{dQ}{dt} \tag{19}$$

where L is the inductance value, which can be calculated from the fluid density and the geometry of the flow conduit:

$$L = \rho l/A \tag{20}$$

where l and A are the length and the cross-sectional area of the conduit.

Assembled Windkessel Module and Corresponding Analytical Model

We assembled the Windkessel impedance module by putting together two resistors and one capacitor as shown in Fig. 5a. Note that in such a physical setup the reference pressure of the capacitor is the initial pressure within the capacitor when the system is in no-flow equilibrium, and thus the capacitor is considered to be connected to the "ground". In the analytical model, inductive effects of the fluid body is taken into account[14] and the impedance module is represented as an LRCR circuit as shown in Fig. 5b. Note that even though there is an inductance associated with the downstream resistance R_d, since the flow through R_d is typically nearly constant, the presence of the inductance is transparent to the operation of the impedance unit. Incorporating only the upstream inductance in the analytical model is sufficient to fully capture the behavior of the physical impedance module.

EXPERIMENTAL TESTING AND DATA ANALYSIS

Resistance Module

We tested the operation of the resistance modules with a setup depicted in Fig. 6. We used a 1/12 horsepower, 3,100 RPM, steady flow pump (Model 3-MD-HC, Little Giant Pump Co., OK) to drive flow through the resistance module. The working fluid in the flow system was a 40% glycerol solution with a dynamic viscosity similar to that of blood. For data acquisition, we used an ultrasonic transit-time flow probe to monitor the flow through the system. We placed the externally clamped flow probe (8PXL, Transonic

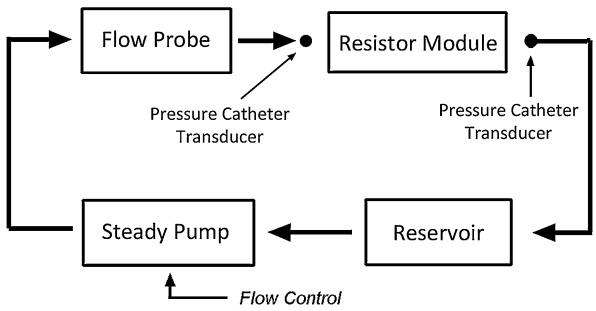

FIGURE 6. Resistance module steady flow testing setup.

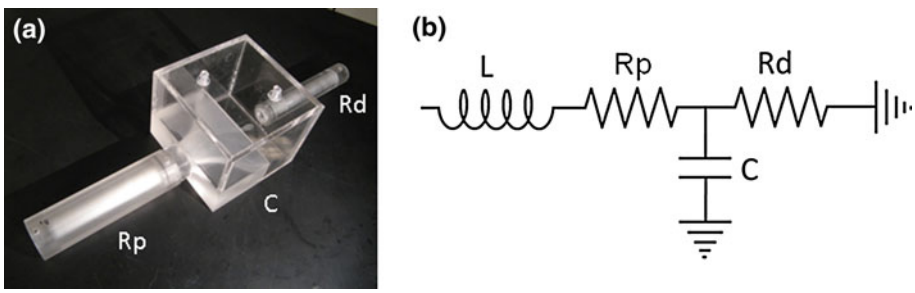

FIGURE 5. (a) Assembled impedance module. (b) Final analytical model of impedance module.

Systems, NY) around a short section of Tygon tubing R3603, and sent the signals from the probe into a flowmeter (TS410, Transonic Systems, NY). For pressure measurements, we inserted catheter pressure transducers ("Mikro-Tip" SPC-350, Millar Instruments, Huston, TX) into the flow conduit immediately upstream and downstream of the resistance module to capture instantaneous pressure readings, and obtain the pressure drop across the resistor. We sent the signals from each catheter pressure transducer into a pressure control unit (TCB-600, Millar Instruments, TX) which produces an electrical output of 0.5 V per 100 mmHg of pressure. We recorded the data from the flow meter and the pressure control units at a sample rate of 2 kHz using a data acquisition unit (USB-6259, National Instruments, Austin, TX) and a LabVIEW program (LabVIEW v.8, National Instruments, Austin, TX). We averaged 8,000 samples of flow and pressure (effectively, 4 s of flow and pressure) to obtain each data point. We then divided the measured pressure drop across the resistor by the measured volumetric flow rate through the resistor to obtain the resistance value.

The flow control for the steady pump consisted of a LabVIEW program that directed the data acquisition unit to send a voltage to an isolation amplifier (AD210, Analog Devices, MA), which then produced the same control voltage to feed into a variable frequency drive (Stratus, Control Resources Inc., MA) that drove the flow pump to produce different constant flow rates through the flow loop. The purpose of including the isolation amplifier in the signal chain was to electronically de-couple the high-power operation of the variable frequency pump drive from the data acquisition unit to avoid signal interference.

In addition to the resistance modules, we also tested the resistance of a partially closed ball valve, which has commonly been used as a method to produce flow resistance in previous literatures.[4,6] We adjusted the relative resistance of the ball valve by adjusting the proportion that the valve was closed.

Assembled Windkessel Module

We tested the assembled Windkessel impedance modules using a setup depicted in Fig. 7. A custom-built, computer-controlled pulsatile pump in parallel with a steady flow pump produced physiological-level, pulsatile, and cyclic flow waveforms into the Windkessel module. Two ultrasonic transit-time flow probes (8PXL & 6PXL, Transonic Systems, NY) were used to monitor the volumetric flows through R_p and R_d. For pressure measurements, we inserted catheter pressure transducers into the flow conduits and into the capacitor chamber to capture the pressure waveforms at three points in the circuit. The flow and pressure data were recorded at a sample rate of 96 samples per second. We averaged approximately 50 cycles of flow and pressure data to obtain one representative cycle of flow and pressure waveforms. We used the pressures measured at P3 as the ground reference, and subtracted it from the pressures measured at P1 and P2, to obtain the true pressure waveforms at P1 and P2.

We tested two impedance modules, one mimicking the *in vivo* thoracic–aortic impedance, and the other mimicking the *in vivo* renal impedance, using four different input flow waveforms approximately simulating physiological flows for each module. We included input flow waveforms with different periods, as well as considerably different shapes, to investigate the impedance behavior of each module across a wide range of flow conditions.

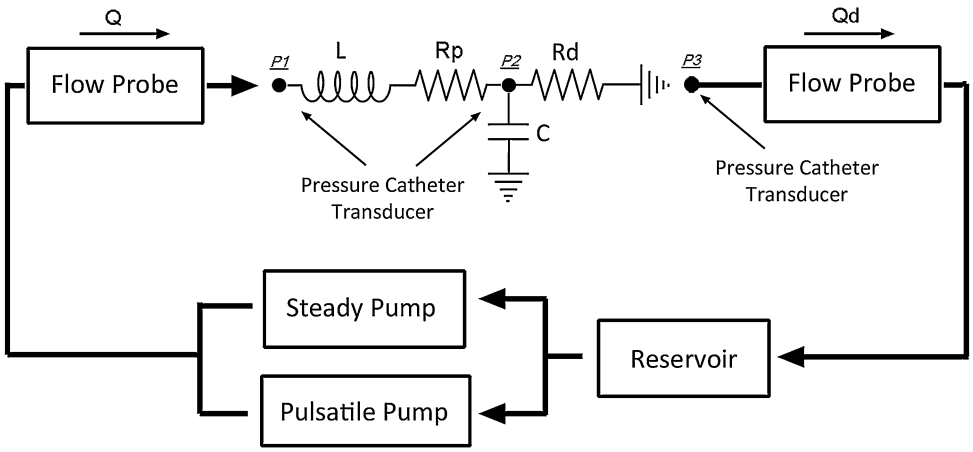

FIGURE 7. Impedance module pulsatile flow testing setup.

The impedance of the analytical Windkessel circuit in Fig. 7 can be represented by the equation:

$$Z(\omega) = j\omega L + R_p + \frac{R_d}{1 + j\omega C R_d} \quad (21)$$

By prescribing the measured input flow waveform, and the values of the lumped components, we calculated the theoretical pressure waveform at P1 using Eqs. (1) and (21). We then calculated the theoretical pressure waveform at P2 and the flow waveform Q_d using the equation $\Delta P = QR$.

RESULTS AND DISCUSSIONS

Resistance Module

Figure 8 presents results of resistance vs. flow rate for two of the resistance modules, and for a partially closed ball valve. In Fig. 8a, the theoretical resistance of the resistance module is 500 Barye s/cm^3. The measured resistance is very close to the expected theoretical value, and the resistance module exhibits relatively constant resistance values over the range of flow rates tested. The variation in the resistance value between flow rates of 20 and 100 cc/s is approximately 5%. The ball valve on the other hand, exhibits a resistance that varies linearly with the flow rate. Figure 8b shows results of a resistance module with theoretical resistance of 6,700 Barye s/cm^3, and a ball valve adjusted to produce a higher flow resistance. We see similar results at this higher regime of resistance values. The value variation of the resistance module between flow rates of 20 and 60 cc/s is approximately 7%. Note that a resistance unit with resistance in the higher regime typically only needs to accommodate relatively low flows in its actual operation. If placed within a Windkessel module under physiologic flows, the expected maximum flow through such a resistor in Fig. 8b would be approximately 30 cc/s. All of the other resistor modules we have tested (but not shown here) also exhibited similar behaviors of relatively constant resistance values over the range of flow rates they are expected to accommodate. The resistance of the ball valve showing a linear dependence on flow rate, and extrapolated value of zero at zero flow, suggests that it is a result of turbulence alone as discussed in "Flow Resistance Module" section. For the resistance modules, the slight increases in the resistance value with flow rate suggest that there is a small amount of turbulence present in the modules.

The resistance variations at the low flow regions are likely due to measurement imprecision, but not due to the actual resistance change or instability in the resistance module. Very low flows and small pressure drops across the resistor result in low signal-to-noise for both the ultrasonic flow probe and the pressure transducers, and hence difficulties in obtaining precise measurements. Fortunately, the fact that the pressure drop across the resistor is insignificant during very low flows, means that the resistance value also have minimal impact during that period. The accuracy of experimental confirmation of resistance values during the very low flow regions is thus of minimal importance.

At a fixed flow rate, we found that the resistance value of a resistance module may decrease over time by up to 5%. The decrease may be due to trapped air bubbles being purged out of the capillary tubes over time with flow (since the presence of air bubbles in the tubes would obstruct the fluid passage and result in elevated resistance). This source of resistance variation can be minimized with careful removal of air from the

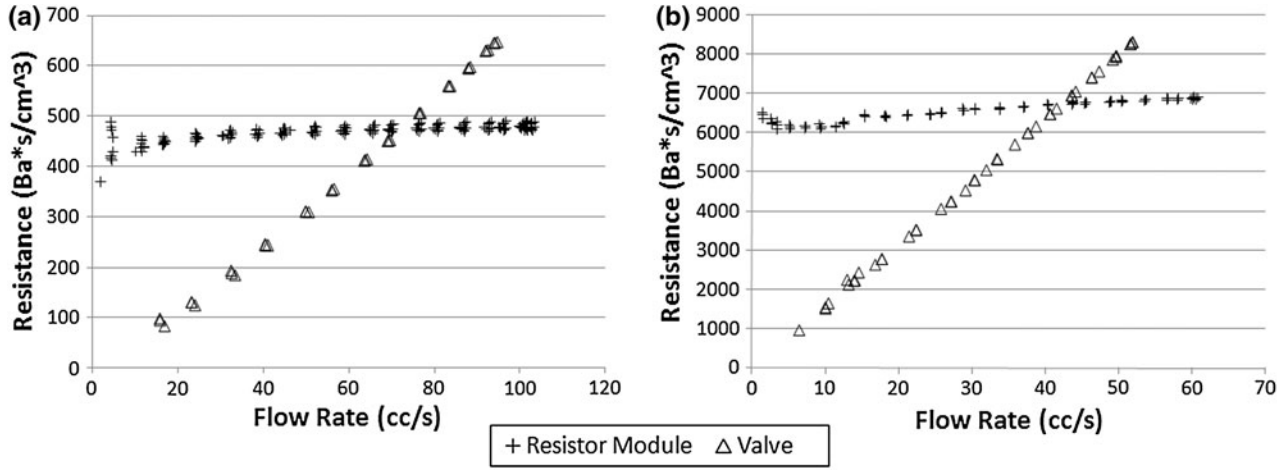

FIGURE 8. Resistance vs. flow rate for resistance module with theoretical resistance of (a) 500 Barye s/cm^3, (b) 6,700 Barye s/cm^3, and a partially closed ball valve.

flow system during setup to minimize the amount of air that would be trapped in the resistor during operation.

Assembled Windkessel Module

Table 2 shows the theoretical Windkessel component values as calculated from their physical constructions, where the values of L calculated from the geometry of the physical system as described in "Flow Inductance" section, the values of resistances calculated from their construction details as described in "Flow Resistance Module" section, and the values of C calculated from the operating pressure and air volume in the capacitors as described in "Flow Capacitance Module" section. The experimental component values in Table 2, unless otherwise noted, were determined from the experimentally measured pressure and flow data, using a method similar to that described in "Determining Target Windkessel Component Values" section. For the thoracic–aortic impedance module, the inductance and resistances behaved as theoretically predicted, where the observed capacitance in the actual experiment was larger than the theoretical expectation. For the renal impedance module, we experimentally determined the resistance values from steady flow tests of the impedance module, and found that the actual resistances were about 15% less than theoretical. The inductance value, on the other hand, was higher than theoretical. The capacitance value was consistent with the theoretical prediction. The differences between the theoretical and experimental component values may be attributed to variations in the physical construction of the components, as well as to the connection parts in between the components.

We prescribed the experimental component values from Table 2 in the analytical calculations of pressure and flow. Figure 9 shows pressure and flow comparisons between experimental measurements and analytical calculations for the impedance module mimicking the *in vivo* aortic impedance at the thoracic level. For all of the four different input flow waveforms tested, the measured pressure waveforms at P1 and P2 (as denoted in Fig. 7), and the flow waveform through R_d, all agree extremely well with the analytical calculations in their shapes, phases, and magnitudes. The maximum difference between measured and calculated pressure (P1 & P2) and flow (Q_d) is 6 and 8%, respectively. Note that two different cyclic periods (1 and 0.75 s) were included in the test and analysis, and the impedance module performed predictably under flow conditions with both period lengths. Figure 10 shows similar results for the impedance module mimicking the renal impedance. There is the same excellent match between experimental measurements and analytical calculations of pressure and flow waveforms for all of the four different flow conditions tested. The maximum difference between measured and calculated pressure (P1 & P2) and flow (Q_d) is 8 and 15%, respectively.

In Figs. 9 and 10, the flow waveforms show that much of the pulsatility in the input flow is absorbed by the capacitor, and the flow through the downstream resistor is fairly constant. This implies that for any given input flow waveform, the proximal resistor R_p needs to be able to accommodate the peak flow of the input waveform, where the downstream resistor R_d only needs to accommodate approximately the averaged flow of the input waveform.

By subtracting Q_d from Q, we can calculate the flow into the capacitor, which then can be integrated to find the change in fluid volume inside the capacitor over each cardiac cycle. From calculations of pressure and volume with Eq. (15), we confirmed that the variation of capacitance value due to the volume change over each cardiac cycle is less than 3% from the reference value for both impedance modules.

Figure 11 shows the impedance modulus and phase as derived from the analytical model, and as calculated from the four sets of experimental pressure and flow data for each module. For both impedance modules, there is close agreement between the theoretical impedance modulus and phase, and those determined from the experimental data of all of the four different flow conditions. This further shows that the impedance modules behave very consistently even when the flow conditions were changed. The general shapes and

TABLE 2. Theoretical and experimental Windkessel component values for the thoracic–aortic and renal impedance modules.

	Thoracic–aortic		Renal	
	Theoretical	Experimental	Theoretical	Experimental
L (Barye s^2/cm^3)	7	7	16	26
R_p (Barye s/cm^3)	245	245	3,050	2,522
C (cm^3/Barye)	2.3 e−4	4.0 e−4	1.3 e−4	1.3 e−4
R_d (Barye s/cm^3)	4,046	4,046	5,944	5,221

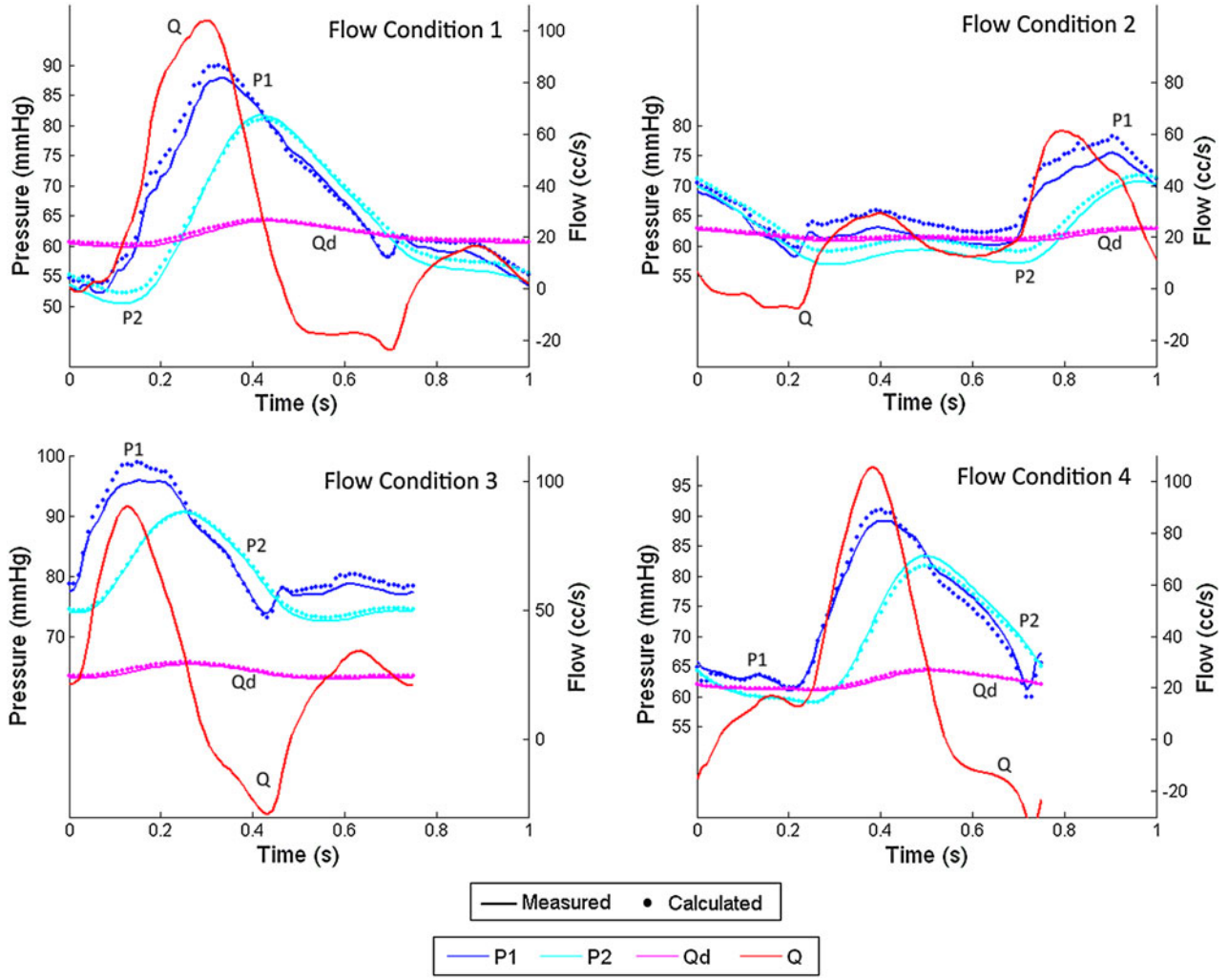

FIGURE 9. Comparisons between measured (*solid lines*) and calculated (*dots*) pressure and flow waveforms for the thoracic–aortic impedance module under four different flow conditions. Note that P1, P2, Q_d, and *Q* are the pressures and flows in the impedance module as depicted in Fig. 7.

magnitudes of the impedance modulus and phase also compare well with those measured *in vivo* in previous studies.[10,14,17,18]

CONCLUSION

We showed that using the methods presented here, we can construct flow resistance units with stable resistance values over wide ranges of flow rates. This is a significant advancement from the common practice of using a partially closed valve to create flow resistances. The resistance value of the units we constructed can both be theoretically determined from construction details, and experimentally confirmed from pressure and flow measurements. We further showed that the impedance module assembled from individual resistor and capacitor components performs very consistently across different flow conditions, and that the corresponding analytical model faithfully captures the behavior of the physical system. When actually employing the physical Windkessel module in other experimental applications, whenever possible, flow and pressure data should be used to confirm or adjust the lumped component value assignments in the corresponding analytical model. We have shown that upon proper characterization of a particular impedance module, the analytical model can then accurately predict its behavior under different flow conditions.

Compared to the Windkessel module previously presented by Westerhof *et al.*,[17] the methods presented here offer simpler and more robust construction, and include considerations for minimizing turbulence in order to minimize parasitic resistances and resistance

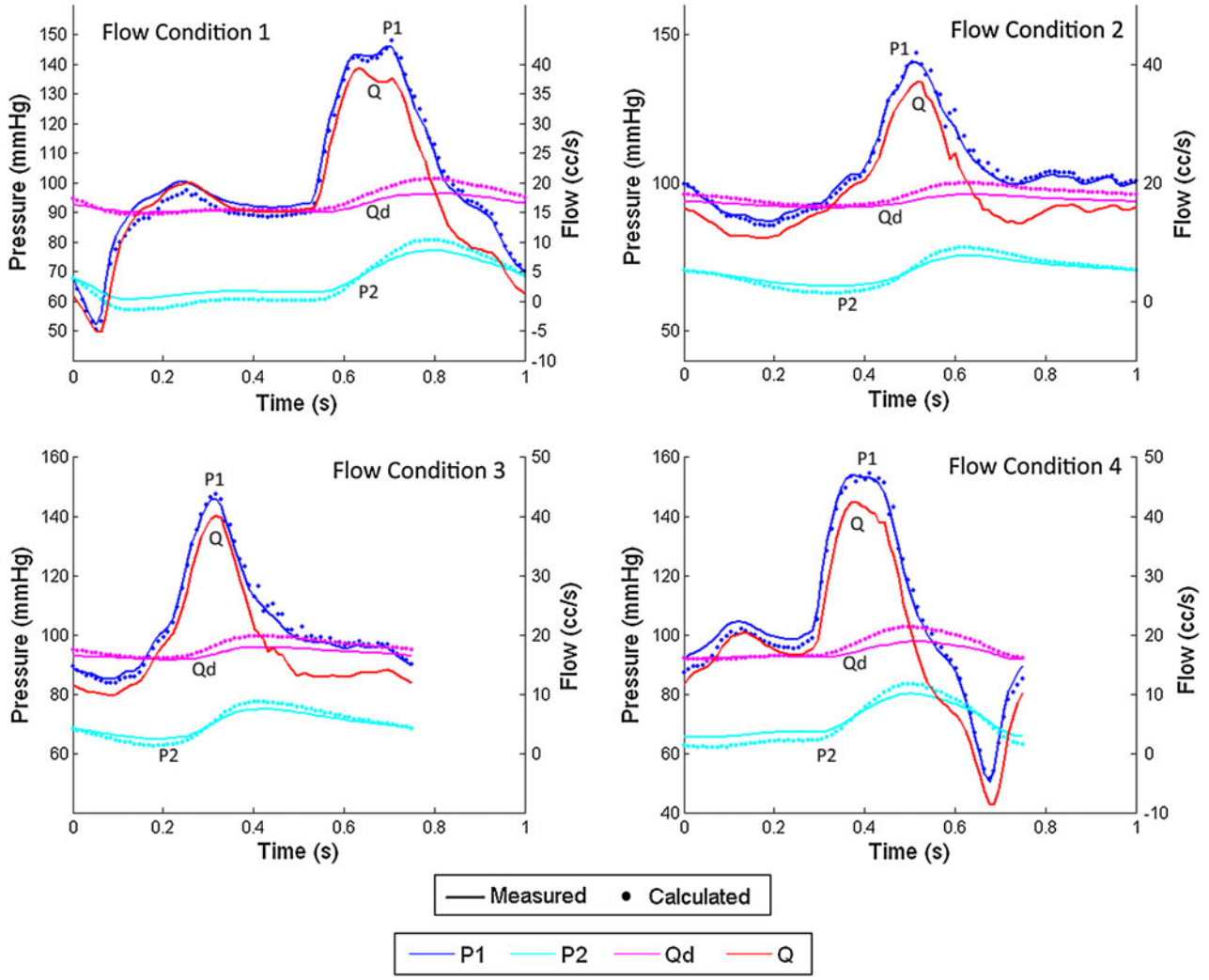

FIGURE 10. Comparisons between measured (*solid lines*) and calculated (*dots*) pressure and flow waveforms for the renal impedance module under four different flow conditions. Note that P1, P2, Q_d, and Q are the pressures and flows in the impedance module as depicted in Fig. 7.

variations across different flow rates. The analytical model presented here also includes the physical effects of inductance, offering a more complete description of the physical system.

In conclusion, the Windkessel impedance module we developed can be used as a practical tool for *in vitro* cardiovascular studies. Implementing the Windkessel module in a physical setup enables the experimental system to replicate realistic blood pressures under physiologic flow conditions. The ability to construct *in vitro* physical systems to mimic *in vivo* conditions can aid in the direct physical testing of implantable cardiovascular medical devices such as stents and stent grafts, and enable reliable measurements of how the *in vivo* forces and tissue motions will interact with the devices. In the area of CFD validation, well-characterized physical Windkessel modules connected to the outlets of a physical phantom will allow prescriptions of the same outlet boundary condition in the computational domain, such that the boundary condition prescription *in silico* is representative of the physical reality. Furthermore, the ability to implement realistic impedances *in vitro* enables experimental studies involving deformable materials, where realistic pressures are absolutely essential for obtaining proper fluid–solid interactions. These studies will be useful for investigating the pulsatile motions of blood vessels, and wave propagations in the cardiovascular system. The work presented here serves as a basis to contribute towards more rigorous cardiovascular *in vitro* experimental studies in the future.

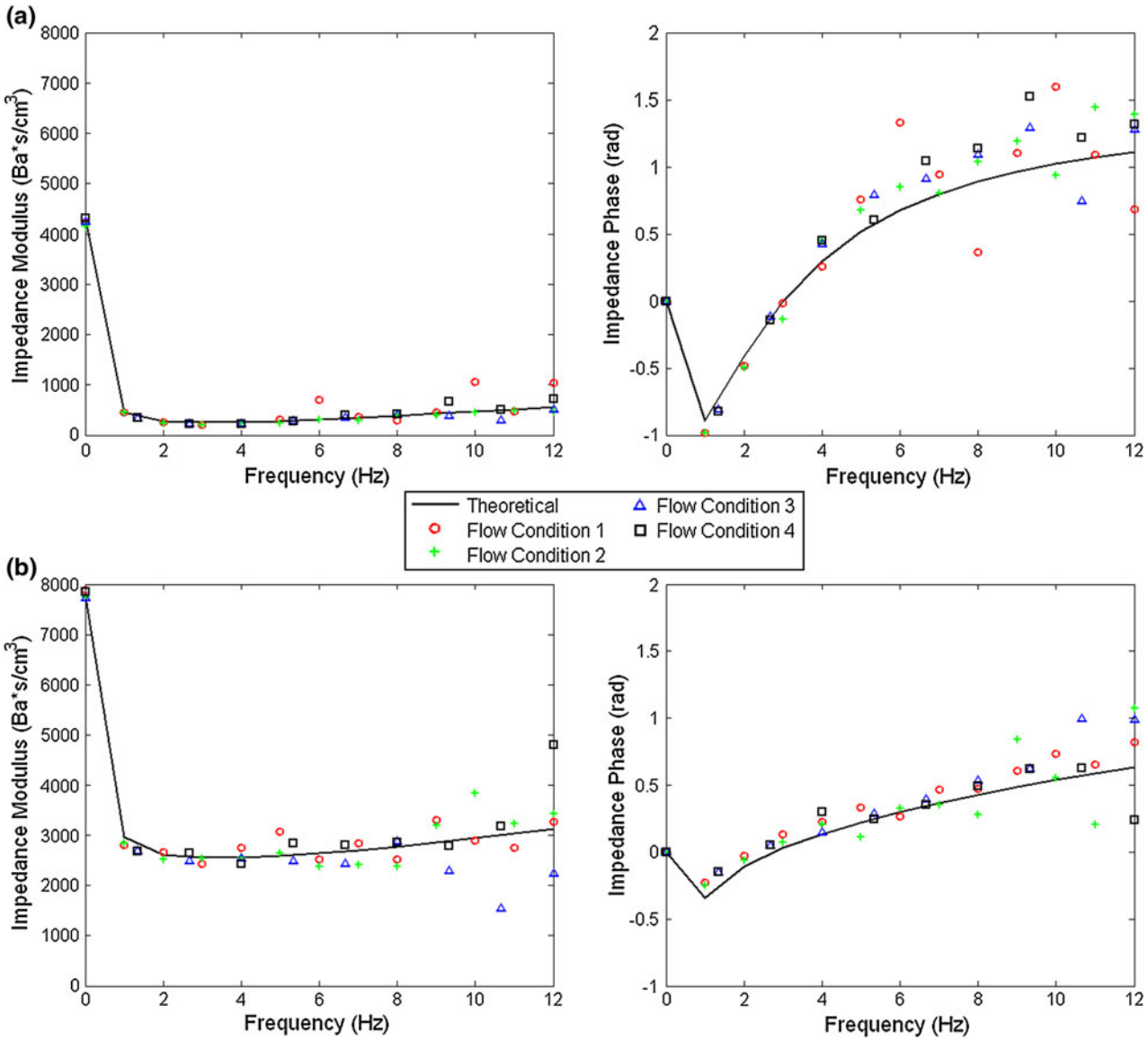

FIGURE 11. Comparisons between theoretical and experimental flow impedance modulus and phase for the (a) thoracic–aortic, and (b) renal, impedance module.

ACKNOWLEDGMENTS

The authors would like to thank Lakhbir Johal and Chris Elkins for assistance with the physical construction of the Windkessel modules and with the flow experiments. This work was supported by the National Institutes of Health (grants P50 HL083800, P41 RR09784, and U54 GM072970).

REFERENCES

[1]Bax, L., C. J. Bakker, W. M. Klein, N. Blanken, J. J. Beutler, and W. P. Mali. Renal blood flow measurements with use of phase-contrast magnetic resonance imaging: normal values and reproducibility. *J. Vasc. Interv. Radiol.* 16(6):807–814, 2005. doi:16/6/807[pii]10.1097/01.RVI.0000161144.98350.28.

[2]Grant, B. J., and L. J. Paradowski. Characterization of pulmonary arterial input impedance with lumped parameter models. *Am. J. Physiol.* 252(3 Pt 2):H585–H593, 1987.

[3]Greene, E. R., M. D. Venters, P. S. Avasthi, R. L. Conn, and R. W. Jahnke. Noninvasive characterization of renal artery blood flow. *Kidney Int.* 20(4):523–529, 1981.

[4]Khunatorn, Y., R. Shandas, C. DeGroff, and S. Mahalingam. Comparison of in vitro velocity measurements in a scaled total cavopulmonary connection with computational predictions. *Ann. Biomed. Eng.* 31(7):810–822, 2003.

[5]Krenz, G. S., J. H. Linehan, and C. A. Dawson. A fractal continuum model of the pulmonary arterial tree. *J. Appl. Physiol.* 72(6):2225–2237, 1992.

[6]Ku, J. P., C. J. Elkins, and C. A. Taylor. Comparison of CFD and MRI flow and velocities in an in vitro large artery bypass graft model. *Ann. Biomed. Eng.* 33(3):257–269, 2005.
[7]Lagana, K., R. Balossino, F. Migliavacca, G. Pennati, E. L. Bove, M. R. de Leval, *et al.* Multiscale modeling of the cardiovascular system: application to the study of pulmonary and coronary perfusions in the univentricular circulation. *J. Biomech.* 38(5):1129–1141, 2005. doi:10.1016/j.jbiomech.2004.05.027.
[8]Les, A. S., S. C. Shadden, C. A. Figueroa, J. M. Park, M. M. Tedesco, R. J. Herfkens, *et al.* Quantification of hemodynamics in abdominal aortic aneurysms during rest and exercise using magnetic resonance imaging and computational fluid dynamics. *Ann. Biomed. Eng.* 38(4):1288–1313, 2010. doi:10.1007/s10439-010-9949-x.
[9]Lotz, J., C. Meier, A. Leppert, and M. Galanski. Cardiovascular flow measurement with phase-contrast MR imaging: basic facts and implementation. *Radiographics* 22(3):651–671, 2002.
[10]Segers, P., S. Brimioulle, N. Stergiopulos, N. Westerhof, R. Naeije, M. Maggiorini, *et al.* Pulmonary arterial compliance in dogs and pigs: the three-element Windkessel model revisited. *Am. J. Physiol.* 277(2 Pt 2):H725–H731, 1999.
[11]Specht, E. Packomania. In: The Best Known Packings of Equal Circles in the Unit Circle. Germany: University of Magdeburg, 2010, http://www.packomania.com/cci. Accessed 5 May 2010.
[12]Spilker, R. L., J. A. Feinstein, D. W. Parker, V. M. Reddy, and C. A. Taylor. Morphometry-based impedance boundary conditions for patient-specific modeling of blood flow in pulmonary arteries. *Ann. Biomed. Eng.* 35(4):546–559, 2007. doi:10.1007/s10439-006-9240-3.
[13]Steele, B. N., M. S. Olufsen, and C. A. Taylor. Fractal network model for simulating abdominal and lower extremity blood flow during resting and exercise conditions. *Comput. Methods Biomech. Biomed. Eng.* 10(1):39–51, 2007. doi:770213688[pii]10.1080/10255840601068638.
[14]Stergiopulos, N., B. E. Westerhof, and N. Westerhof. Total arterial inertance as the fourth element of the Windkessel model. *Am. J. Physiol.* 276(1 Pt 2):H81–H88, 1999.
[15]Vignon-Clementel, I. E., C. A. Figueroa, K. E. Jansen, and C. A. Taylor. Outflow boundary conditions for three-dimensional finite element modeling of blood flow and pressure in arteries. *Comput. Methods Appl. Mech. Eng.* 195(29–32):3776–3796, 2006. doi:10.1016/j.cma.2005.04.014.
[16]Wang, J. J., J. A. Flewitt, N. G. Shrive, K. H. Parker, and J. V. Tyberg. Systemic venous circulation. Waves propagating on a Windkessel: relation of arterial and venous Windkessels to systemic vascular resistance. *Am. J. Physiol. Heart Circ. Physiol.* 290(1):H154–H162, 2006. doi:00494.2005[pii]10.1152/ajpheart.00494.2005.
[17]Westerhof, N., G. Elzinga, and P. Sipkema. An artificial arterial system for pumping hearts. *J. Appl. Physiol.* 31(5):776–781, 1971.
[18]Westerhof, N., J. W. Lankhaar, and B. E. Westerhof. The arterial Windkessel. *Med. Biol. Eng. Comput.* 47(2):131–141, 2009. doi:10.1007/s11517-008-0359-2.